

25 **1. Introduction**

26 The magnitude of the aerosol indirect radiative forcing is poorly constrained in climate
27 models, and this is the dominant uncertainty in assessing climate change [IPCC, 2007]. The
28 aerosol indirect radiative forcing is largely determined by the number abundance of particles that
29 can act as cloud condensation nuclei (CCN) [e. g, Twomey, 1977; Albrecht 1989]. New particle
30 formation, which has been frequently observed throughout the troposphere [Kulmala et al.,
31 2004a; Yu et al., 2008], is an important source of atmospheric CCN. To accurately assess the
32 influences of aerosols on climate, interpret past climate, and project future changes, the
33 contribution of secondary particle formation and growth to CCN abundance have to be
34 understood and properly incorporated in the large scale models. In this regard, it is critical to
35 achieve a clear physical understanding of atmospheric particle nucleation mechanisms,
36 especially the dependence of nucleation rates on key atmospheric parameters.

37 Based on an up-to-date kinetically consistent ion-mediated nucleation model (IMN)
38 incorporating recently available thermodynamic data and schemes, Yu [2006] showed that ions
39 can lead to significant particle formation not only in the upper troposphere but also in the lower
40 troposphere (including boundary layer). The involvement of ions in many boundary layer
41 nucleation events has been confirmed by measurements of the evolution of charged clusters
42 during nucleation events and the observed overcharge of freshly nucleated nanometer-sized
43 particles [Iida et al., 2006; Hirsikko et al., 2007; Laakso et al., 2007; Gagné et al., 2008]. Both
44 three-year records of ion mobility measurements [Hirsikko et al., 2007] and one-year
45 overcharging ratio measurements for freshly nucleated particles [Gagné et al., 2008] indicate that
46 ions are involved in more than 90% of the particle formation events that can be clearly identified,
47 although the relative contribution of ion and neutral nucleation remains controversial [see

48 Section 2.2 for more discussion on this]. Detailed case studies [Yu and Turco, 2008] indicate
49 that, for most of well-defined nucleation events observed in Hyytiälä, Finland, the predictions
50 based on the ion-mediated nucleation (IMN) model are in good agreement with field data for a
51 range of variables, including critical nucleation sizes, size-dependent overcharging ratios, and the
52 concentrations of 1.8-3 nm stable clusters and 3-6 nm particles, as well as their diurnal
53 variations. Thus, we have experimental evidence that IMN may be important in the atmosphere.

54 In this paper we study the dependence of IMN rates on key parameters and derive an IMN
55 look-up table from the detailed kinetic IMN model. An overview of the IMN mechanism is given
56 in section 2. The dependence of IMN rates on key parameters and associated implications are
57 discussed in Section 3. Section 4 describes the IMN look-up table, which can be used for a quick
58 and accurate calculation of IMN rates at given conditions. Lastly, section 5 is the summary.

59

60 **2. Overview of ion-mediated nucleation (IMN) mechanism**

61 **2.1. The kinetic IMN model: Physics, features, and recent development**

62 Ions, which are generated continuously and ubiquitously in the atmosphere by cosmic
63 radiation and radioactive decay, have long been suggested to promote nucleation [Castleman *et*
64 *al.*, 1978; Arnold, 1980; Chan and Mohnen, 1980; Hamill *et al.*, 1982; Raes *et al.*, 1986]. Yu and
65 Turco [1997, 2000, 2001] developed a comprehensive approach for studying nucleation
66 processes involving ion clusters. They utilized a kinetic model that explicitly treats the complex
67 interactions among small air ions, neutral and charged clusters of various sizes, precursor vapor
68 molecules, and pre-existing aerosols. Compared to homogeneous nucleation, which involves the
69 formation of small, transient neutral molecular clusters, nucleation onto ions is favored because:
70 (1) small charged clusters are typically much more stable thermodynamically than their neutral
71 counterparts [Yu, 2005, 2006]; (2) the initial growth rates of small ion clusters are enhanced by

72 the dipole-charge interaction between the core ion and the strongly dipolar condensing molecules
73 [*Nadykto and Yu, 2003*]; and (3) there is a continuous and ubiquitous supply of stable, fast
74 growing ionic embryos. *Yu and Turco [2000]* refer to the coupled formation and evolution of
75 cluster size distributions, including both charged and neutral clusters, under the influence of
76 ionization, recombination, neutralization, condensation, evaporation, coagulation, and
77 scavenging as ion-mediated nucleation (IMN).

78 The IMN theory differs substantially from classical ion-nucleation theory, which is
79 commonly adopted in the literature [e.g., *Hamill et al., 1982; Raes et al., 1986; Laakso et al.,*
80 *2003*]. Classical “ion-nucleation” is based on a simple modification of the free energy associated
81 with the formation of a “critical nucleation embryo” in which the electrostatic potential energy
82 induced by the embedded charge is included. However, this classical approach does not properly
83 account for the kinetic limitation to embryo development imposed by the typically low
84 atmospheric concentrations of precursors, especially sulfuric acid. In addition, the important
85 contribution of neutral clusters resulting from ion-ion recombination to nucleation is not
86 considered in the classical ion-nucleation theory. By contrast, in IMN theory, the kinetic effect of
87 charge on cluster growth rates and the contribution of neutral clusters resulting from the
88 neutralization of charged clusters are explicitly considered.

89 IMN explains the rapid initial growth of small clusters, as a result of the charge-neutral
90 interactions. This initial growth phase (to sizes of ~1.5 nm diameter) is not to be confused with
91 later stages of stable nanoparticle growth (from ~2-3 nm and larger). In the initial phase, ion-
92 molecule interactions greatly accelerate the kinetics of molecular association – by up to an order
93 of magnitude. However, by the time the nucleating embryos are larger than ~ 1.5 nm in diameter,
94 the charge-enhanced growth effect becomes quite small due to the inverse relationship between

95 charge effect and embryo size [*Nadykto and Yu, 2003*] and rapid neutralization of ion embryos
96 [*Yu, 2006; Yu and Turco, 2008*]. Subsequently, the growth rate is dominated by the vapor
97 pressure of the major condensing species. In the case of organic condensates, for example, the
98 normal Kelvin effect would predict that the growth rate accelerates as the particles size increases,
99 opposite to the effect produced by a fixed particle charge. This predicted pattern of growth is
100 consistent with observations [e.g., *Kulmala et al, 2004b*].

101 Built upon an earlier version of the IMN model [*Yu and Turco, 1997, 2000, 2001*], *Yu* [2006]
102 developed a second-generation IMN model which incorporates new thermodynamic data [*Froyd,*
103 2002; *Wilhelm et al., 2004*] and physical algorithms [*Nadykto and Yu, 2003; Yu, 2005*] and
104 explicitly treats the evaporation of neutral and charged clusters. The uncertainty in the IMN
105 model has been further reduced by using two independent measurements to constrain monomer
106 hydration in the H₂SO₄-H₂O system, and by incorporating recently determined energetics of
107 small neutral H₂SO₄-H₂O clusters [*Yu, 2007*]. It should be pointed out that the present IMN
108 model is for the H₂SO₄-H₂O binary system. In the atmosphere, species other than H₂SO₄ and
109 H₂O (such as NH₃, amines, HNO₃, and some organics) may be involved in the IMN process
110 under some conditions. Obtaining necessary thermodynamic data and extending the IMN model
111 for a multiple-component nucleation system will be the subject of future research.

112 Based on the most comprehensive and well-constrained case studies of atmospheric
113 nucleation processes to date (at least to our knowledge), *Yu and Turco* [2008] concluded that,
114 beyond a reasonable level of uncertainty, IMN appears to be the dominant nucleation mechanism
115 in at least a large fraction of nucleation events observed during an intensive field campaign in
116 boreal forests. In addition, the global nucleation spatial patterns and absolute magnitude
117 predicted using the IMN mechanism is reasonably consistent to land-, ship-, and aircraft-based

118 observations [Yu *et al.*, 2008]. More recently, Yu and Luo [2009] used global size resolved
119 aerosol microphysics modeling to show that IMN is able to account for (within a factor of two)
120 the annual mean particle number concentrations observed in many parts of troposphere.

121

122 **2.2. Controversy with regard to the importance of IMN in the atmosphere**

123 While our analyses indicate that the ion mobility data and the measurements of excess charge
124 on freshly nucleated particles in the boreal forest support the dominance of the IMN mechanism
125 [Yu and Turco, 2007, 2008], Kulmala and colleagues concluded that, based on their analysis of
126 the same dataset, IMN contributes only up to ~ 10% to the boreal forest nucleation [Laakso *et al.*
127 *et al.*, 2007; Kulmala *et al.*, 2007; Gagné *et al.*, 2008; Boy *et al.*, 2008; Manninen *et al.*, 2009].
128 Given such discrepancies, we discuss these studies here along with possible reasons for the
129 differences.

130 Kulmala and colleagues' studies concluding the dominance of neutral nucleation process
131 include: (1) Laakso *et al.* [2007] and Gagné *et al.* [2008] extrapolated measured charging states
132 of nucleation mode particles (~ 3 - 7 nm) down to smaller sizes (1-2 nm) and concluded that the
133 contribution of IMN to total nucleation rate was either negligible or relatively small in a large
134 fraction of days considered. (2) Kulmala *et al.* [2007] and Manninen *et al.* [2009] calculated the
135 formation rate of total and charged 2 nm particles from the particle concentrations detected in the
136 size range of ~2–3 nm, and concluded that IMN contributes ~ 10% to the boreal forest new
137 particle formation events. (3) Boy *et al.* [2008] simulated 4 days of nucleation events using
138 atmospheric input data from the SMEAR II station. They calculated the IMN rate based on the
139 model of Kazil and Lovejoy [2007], and used the empirical activation ($J_{\text{act}} = A [\text{H}_2\text{SO}_4]$) and
140 kinetic nucleation formulas ($J_{\text{kin}} = K [\text{H}_2\text{SO}_4]^2$) to represent neutral nucleation. By comparing
141 their calculated ion and neutral nucleation rates, Boy *et al.* [2008] concluded that IMN

142 contributes between <0.5 to 12% to the total number of particles nucleated inside the mixed layer
143 in the boreal forests.

144 Yu and Turco's studies pointing out the dominance of the IMN process include: (1) *Yu and*
145 *Turco* [2007] showed, based on a conservative analytical analysis of the neutralization of
146 charged particles, that the observed charging states of nucleated particles (~ 3 - 7 nm) reported in
147 *Laakso et al.* [2007] are fully consistent with the dominance of IMN in most of the nucleation
148 events. (2) Based on the well-constrained case studies of nucleation events characterized in
149 Hyytiälä, with a kinetic nucleation model accounting for the size-dependent microphysics of
150 neutral and charged clusters, *Yu and Turco* [2008] demonstrated a good agreement between the
151 IMN predictions and field data for a wide range of the key parameters including the
152 overcharging ratio (OR) of 3-7 nm particles and concluded that IMN is likely to be the dominant
153 nucleation mechanism in at least a large fraction of nucleation events in boreal forests.

154 One possible cause of such different conclusions is that Kulmala and colleagues' analyses
155 focused on 2-3 nm particles while Yu and Turco's kinetic modeling considered the actual
156 dynamics of the formation of clusters with diameters ranging from ~0.5 nm to >3 nm. Kulmala
157 and colleagues assume that all neutral particles ~ 2 nm or growing into 2 nm are from neutral
158 nucleation. This may lead to significant underestimation of the IMN contribution because a
159 significant fraction of neutral particles ~ 2 nm and smaller may be formed from the IMN [*Yu and*
160 *Turco*, 2008]. *Yu et al.* [2007] have demonstrated that *Laakso et al.* [2007]'s conclusion that
161 IMN has a negligible or small contribution to new particle formation is inconsistent with their
162 own analysis of the charging state (Sc) of 1 nm particles. *Laakso et al.* [2007]'s conclusion
163 appears to be based on Sc values of 2 nm particles. However, it is more appropriate to use Sc at 1
164 nm because neutral particles at 1-2 nm may actually be produced by the neutralization of

165 particles formed on ions and thus are a direct result of IMN [Yu and Turco, 2008]. Based on Sc
166 at 1 nm given in *Laakso et al.* [2007], a large fraction (60%) of the days have either a significant
167 or dominant ($Sc > 50$) contribution from IMN, while only a small fraction (13%) of days have
168 either negligible ($Sc < 1$) or small ($Sc < 10$) contributions from IMN [Yu et al., 2007]. These
169 considerations lead us to conclude that *Laakso et al.*'s analysis may actually support Yu and
170 Turco's conclusion. Similarly, we think that *Kulmala et al.* [2007] and *Manninen et al.* [2009]
171 underestimated the importance of IMN because they assumed all neutral particles growing to ~ 2
172 nm were produced via neutral nucleation, while in the reality these particles may have been
173 formed via the neutralization of particles formed on ions. The conclusion of *Boy et al.* [2008] is
174 not surprising because they used the ion nucleation model similar to that of *Lovejoy et al.* [2004],
175 which under-predicts ion nucleation rate by several orders of magnitude [Yu and Turco, 2008]. In
176 addition, *Boy et al.* [2008] used empirical activation and kinetic nucleation formulas to represent
177 neutral nucleation. It remains to be established whether the empirical formula indicates a new
178 nucleation mechanism or if it simply represents an empirical fitting of existing nucleation process
179 such as IMN [Yu and Turco, 2008].

180 While more comprehensive studies are needed in order to more clearly resolve the IMN
181 controversy, our analyses given above indicate that Kulmala and colleagues might have
182 underestimated the importance of IMN, and the results of *Laakso et al.* [2007] may actually
183 support the significance of IMN. It should be emphasized that the dominance of the neutral
184 nucleation process will lead to the undercharging of freshly nucleated particles. *Laakso et al.*
185 [2007] and *Gagne et al.* [2008] showed that ion-DMPS detected substantial undercharging of
186 freshly nucleated particles in only $\sim 10\%$ of nucleation event days. The undercharging could be

187 an indication of the dominance of neutral nucleation; however it may also be a result of air mass
188 inhomogeneity and uncertainties in measurements [Yu and Turco, 2008].

189

190 **3. Dependence of IMN rates on key parameters and implications**

191 The IMN model explicitly solves the dynamic equations governing the size distribution
192 evolution of neutral, positively charged, and negatively charged cluster/particles. The IMN rates
193 (denoted as J_{IMN}) are calculated based on the net fluxes of particles across the critical size of
194 neutral embryos. Under a given condition, cluster distribution and nucleation rate reach steady
195 state after a certain amount of time. Detailed information about the IMN model and how IMN
196 rates are determined can be found in Yu [2006]. All the IMN rates presented in this paper are the
197 steady state values, and the steady state apparent IMN rates across the clusters containing 10
198 sulfuric molecules (around 1.5 nm) are used for the conditions that give very small critical size
199 (containing less than 10 sulfuric molecules). The current version of the IMN model only
200 considers the binary $\text{H}_2\text{SO}_4\text{-H}_2\text{O}$ system, and there are five key parameters controlling J_{IMN} :
201 sulfuric acid vapor concentration ($[\text{H}_2\text{SO}_4]$), temperature (T), relative humidity (RH), ionization
202 rate (Q), and surface area of pre-existing particles (S). Figures 1-5 show the dependence of J_{IMN}
203 on these parameters, based on the calculations from full IMN model (solid lines) and IMN look-
204 up table detailed in Section 4 (dashed lines).

205

206 3.1. Sulfuric acid vapor concentration ($[\text{H}_2\text{SO}_4]$)

207 Figure 1 gives J_{IMN} as a function of $[\text{H}_2\text{SO}_4]$ for four different atmospheric states. There is no
208 doubt that $[\text{H}_2\text{SO}_4]$ is a key parameter controlling J_{IMN} . To achieve a nucleation rate of $1 \text{ cm}^{-3}\text{s}^{-1}$
209 under typical values of Q ($10 \text{ ion-pairs cm}^{-3}\text{s}^{-1}$), RH (50%), and S ($100 \mu\text{m}^2 \text{ cm}^{-3}$), $[\text{H}_2\text{SO}_4]$ has
210 to be around 6×10^6 , 9×10^6 , 2.5×10^7 , and 10^8 cm^{-3} for T = 265, 275, 285, and 295 K, respectively.

211 Nucleation events have been frequently observed in boreal forests during the spring season when
212 T is ~270 -285 K and peak $[H_2SO_4]$ is in the range of $5 \times 10^6 - 3 \times 10^7 \text{ cm}^{-3}$. It has been shown by
213 *Yu and Turco* [2008] that the IMN mechanism appears to be able to account for at least a large
214 fraction of these nucleation events and is supported by the observed overcharging of freshly
215 nucleated particles.

216 Under the conditions considered in Fig. 1, J_{IMN} is very sensitive to $[H_2SO_4]$ when $[H_2SO_4]$ is
217 relatively low and J_{IMN} is relatively small, and becomes insensitive at higher $[H_2SO_4]$, because of
218 the limitation of nucleation by ionization rate. For low T, J_{IMN} becomes sensitive to $[H_2SO_4]$
219 when $[H_2SO_4]$ is high (for example, see the curve with T=230 K when $[H_2SO_4] > \sim 2 \times 10^7 / \text{cm}^3$)
220 because of the dominance of binary homogeneous nucleation (BHN) under such conditions. It
221 should be noted that BHN is an integrated part of IMN [*Yu*, 2006].

222 The importance of $[H_2SO_4]$ in controlling J_{IMN} can also be seen from the global spatial
223 distribution of J_{IMN} presented in *Yu et al.* [2008], showing that high nucleation zones are
224 generally confined to high sulfur source regions. The sensitivity of J_{IMN} to $[H_2SO_4]$ implies that
225 future changes in anthropogenic and natural emissions of sulfur species may have important
226 impacts on new particle formation, aerosol abundance, and radiative forcing. For example,
227 *Charlson et al.* [1987] proposed that a warmer climate would increase dimethylsulphide (DMS)
228 emissions which in turn leads to higher formation rates of sulfate aerosols and CCN abundance.
229 The resulting increase in cloud albedo should reflect more sunlight back to space and thus cool
230 the Earth. On the other hand, the pollution controlling strategies aimed to reduce anthropogenic
231 sulfur emissions may significantly decrease aerosol number abundance in the atmosphere and
232 thus diminish the cooling effects of atmospheric aerosols.

233 3.2 Temperature (T)

234 Figure 2 illustrates the dependence of J_{IMN} on T under four different ambient conditions.
235 Similar to $[\text{H}_2\text{SO}_4]$, T has a strong effect on J_{IMN} . Under a variety of conditions given in Fig. 2,
236 J_{IMN} is very sensitive to T when J_{IMN} increases from insignificant ($< \sim 0.01 \text{ cm}^{-3}\text{s}^{-1}$) to significant
237 ($> \sim 1 \text{ cm}^{-3}\text{s}^{-1}$) as T decreases. After J_{IMN} reaches a significant level, further decreases of T (with
238 other parameters fixed) have relatively small effects because nucleation under such conditions is
239 limited by ionization rates. When T is very low, BHN becomes dominant and the nucleation
240 rates become sensitive to T again. Under typical values of Q ($10 \text{ ion-pairs cm}^{-3}\text{s}^{-1}$), $\text{RH}(50\%)$,
241 and S ($100 \mu\text{m}^2 \text{ cm}^{-3}$), to achieve a nucleation rate of $1 \text{ cm}^{-3}\text{s}^{-1}$, T should be around 268, 277,
242 286, and 291 K, for $[\text{H}_2\text{SO}_4]=5\times 10^6$, 10^7 , 3×10^7 , and $6\times 10^7 \text{ cm}^{-3}$, respectively. Clearly, much
243 higher $[\text{H}_2\text{SO}_4]$ is needed to achieve a similar level of nucleation rate at higher temperature.

244 Based on mass-resolved ion cluster distributions measured in the summer of 2002 at an urban
245 site in Atlanta, Georgia, and in the late summer/fall of 2004 at the National Center for
246 Atmospheric Research (NCAR)'s Marshall Field Site, *Eisele et al.* [2006] concluded that ion-
247 induced nucleation was unlikely to have contributed significantly to the new particle formation
248 observed on some days during the study period. Under the atmospheric conditions corresponding
249 to the days that *Eisele et al.* [2006]'s measurements were made ($T > \sim 290 \text{ K}$, $\text{RH} < \sim 40\%$,
250 $[\text{H}_2\text{SO}_4] < \sim 3\times 10^7/\text{cm}^3$), the IMN model would likewise predict a negligible rate of nucleation
251 ($< 10^{-3}/\text{cm}^3\text{s}$, see Fig. 2). Thus, the IMN mechanism does not directly conflict with these
252 measurements. It is possible that additional species may be involved and enhance nucleation in
253 urban and other disturbed environments. By analyzing the charged fractions (CFs) of 3-5.5 nm
254 particles measured at NCAR's Marshall Field Site, *Iida et al.* [2006] concluded that, while
255 obviously involved in nucleation on some days, ions overall contributed insignificantly to new
256 particle formation observed at the site. Our model predicts negligible IMN rates on days with

257 high temperature ($>\sim 290$ K). However, the model also suggests that IMN can become significant
258 during periods of relatively lower temperatures ($<\sim 285$ K). *Iida et al.* [2006] derived their CFs at
259 1 nm by extrapolating from observed CFs for 3-5.5 nm particles, and the interpretive analysis is
260 likely subject to large uncertainties. For example, during a nucleation period on June 1, 2004, the
261 3-5.5 nm particles were clearly overcharged, with ORs above 2 (Fig. 5 of *Iida et al.*, 2006).
262 Based on our size-dependent kinetic modeling, an OR above 2 for 3-5 nm particles should
263 indicate the dominance of IMN [*Yu and Turco*, 2008], whereas *Iida et al.* [2006] inferred that
264 IMN only contributed $\sim 0.4\%$ of the nucleation. A more detailed case study of measurements
265 reported in *Iida et al.* [2006] may shed new light on the mechanisms of particle nucleation.

266 In the atmosphere, nucleation events typically last for several hours only and there exist clear
267 seasonal variations in the frequency of nucleation events. According to IMN mechanism,
268 temperature and $[\text{H}_2\text{SO}_4]$ are the two most important factors controlling the start and end of
269 nucleation events, although other parameters also contribute to the changes in nucleation rates.
270 The optimum conditions for IMN are relatively high $[\text{H}_2\text{SO}_4]$ and relatively low T, which may
271 explain (at least partially) why nucleation generally occurs in the morning and why nucleation
272 event frequency peaks in the Spring and Fall [e.g., *Stanier et al.*, 2004; *Laaksonen et al.*, 2008].

273 Figure 2 shows that, within the T range that J_{IMN} changes from insignificant ($< \sim 0.01 \text{ cm}^{-3}\text{s}^{-1}$)
274 to significant ($> \sim 1 \text{ cm}^{-3}\text{s}^{-1}$), a 2 K difference in T causes up to around one order of magnitude
275 difference in J_{IMN} . Such high sensitivity of J_{IMN} to temperature may have important implications.
276 For example, future global warming may significantly suppress new particle formation in the
277 atmosphere, reduce CCN abundance and aerosol indirect radiative cooling, and thus may imply a
278 positive climate/nucleation feedback mechanism. The magnitude of this new positive feedback

279 mechanism proposed here should be assessed with global climate models that incorporate the
280 IMN mechanism and proper size-resolved aerosol microphysics.

281 It is also clear from Figure 2 that, at a constant level of $[\text{H}_2\text{SO}_4]$, nucleation is more favored
282 in air with slightly lower temperature. One example is that under some conditions, nucleation is
283 favored in the top of boundary layer instead of surface because of the temperature difference.
284 Actually, many of the nucleation events observed at the surface may be associated with the
285 mixing of particles nucleated aloft (especially particle size distribution evolutions exhibiting the
286 "apple" shape rather than the "banana" shape [Yu *et al.*, 2008]). The high sensitivity of J_{IMN} to T
287 may also imply large inhomogeneities in nucleation rates due to temperature fluctuation in
288 different air masses. Airborne measurements of nucleation-mode aerosol concentrations over
289 boreal forests reveal significant variability in nucleated particle concentrations attributable to
290 variability in land coverage between forests and lakes [O'Dowd *et al.*, 2008], and temperature
291 difference could be one of the factors contributing to the variability.

292 293 3.3 Relative Humidity (RH)

294 The effects of RH on J_{IMN} under four atmospheric conditions are shown in Figure 3. With all
295 other parameters fixed, J_{IMN} increases with increasing RH until J_{IMN} reaches a level that is
296 limited by ionization rates. The effect of RH on J_{IMN} can be very significant under some
297 conditions. For example, J_{IMN} increases by about three orders of magnitude when RH increases
298 (1) from 60% to 90% under one shown condition ($T=290$ K, $[\text{H}_2\text{SO}_4]=2 \times 10^7 \text{ cm}^{-3}$, $Q=10$ ion-pairs
299 $\text{cm}^{-3}\text{s}^{-1}$, and $S=100 \mu\text{m}^2 \text{ cm}^{-3}$) and (2) from 20% to 30% under another condition ($T=285$ K,
300 $[\text{H}_2\text{SO}_4]=5 \times 10^7 \text{ cm}^{-3}$, $Q=10$ ion-pairs $\text{cm}^{-3}\text{s}^{-1}$, and $S=100 \mu\text{m}^2 \text{ cm}^{-3}$).

301 In the real atmosphere, RH has clear diurnal variations which are associated with T changes.
302 The increase of temperature generally leads to the decrease of RH which in turn enhances the

303 effect of T on nucleation rates. *Yu and Turco* [2008] showed in the well-constrained case studies
304 that the increase in T and decrease in RH are the main reasons for the shut-off of nucleation
305 events around noontime observed in boreal forests.

306 Most climate models predict little change in global RH as a result of projected global
307 warming associated with greenhouse effect. Nevertheless, some observations and modeling
308 analysis indicate that RH may decrease as T increases, especially in the middle and upper
309 troposphere [*Minschwaner and Dessler*, 2004]. For each degree of surface warming, absolute
310 RH could decrease 3%–5% in the upper troposphere and 3–10% in the middle troposphere
311 [*Minschwaner and Dessler*, 2004]. The possible decrease in RH associated with global warming
312 could further inhibit the nucleation and thus enhance the positive climate/nucleation feedback
313 mechanism proposed above in section 3.2.

314 It should be noted that RH variations may lead to changes in the surface area of pre-existing
315 particles which is also one of the parameters controlling nucleation rates. Due to the uptake of
316 water by aerosols, an increase in RH will generally increase the size and hence surface area of
317 pre-existing particles, reducing nucleation rates (see Section 3.5 for details). The effect of RH on
318 particle size depends on the composition of particles. To properly assess the combined effects of
319 RH changes on nucleation, a size- and composition- resolved aerosol microphysics model is
320 needed.

321 322 3.4 Ionization rate (Q)

323 The dependence of J_{IMN} on ion production rate is presented in Figure 4 for a number of
324 atmospheric conditions. J_{IMN} is sensitive (almost proportional) to Q when $[\text{H}_2\text{SO}_4]$ is large and Q
325 is relatively low. J_{IMN} generally increases with Q when $[\text{H}_2\text{SO}_4]$ is above around 10^7cm^{-3} .
326 However, J_{IMN} decreases with increasing Q when Q is relatively big and $[\text{H}_2\text{SO}_4]$ is low

327 ($\sim 5 \times 10^6 \text{ cm}^{-3}$). The non-linear dependence of J_{IMN} on Q is a result of the competition between
328 the time needed to grow ion clusters to a stable size (t_g) and the neutralization time (t_n) of
329 charged clusters. The neutralization by ion-ion recombination will cause the growing charged
330 clusters to lose their growth advantage and the resulting neutral clusters may dissociate if smaller
331 than the critical size [Yu, 2006]. t_g is inversely proportional to $[\text{H}_2\text{SO}_4]$ while t_n is inversely
332 proportional to the concentration of small opposite ions ($[\text{ion}]$), which is directly related to Q .

333 The steady-state J_{IMN} is limited by the local ionization rate except under the conditions that
334 BHN becomes dominant. Ambient ions are continuously generated by galactic cosmic rays at the
335 rate of ~ 2 ion-pairs $\text{cm}^{-3}\text{s}^{-1}$ at Earth's surface and up to ~ 20 - 30 ion-pairs $\text{cm}^{-3}\text{s}^{-1}$ in the upper
336 troposphere. Other localized sources (such as radioactive emanations, corona discharge,
337 combustion, lightning, nuclear waste, etc.) can also generate ions. Owing to natural radioactivity
338 from soils, the ionization rate in the continental surface layer can reach up to ~ 10 ion-pairs $\text{cm}^{-3}\text{s}^{-1}$
339 [Reiter, 1992]. Some measurements indicate that ionization rates near the surface can exceed
340 100 ion-pairs $\text{cm}^{-3}\text{s}^{-1}$ due to the accumulation of radon gas in the nocturnal boundary layer
341 [Dhanorkar and Kamra, 1994]. Vartiainen et al. [2007] detected exceptionally high ion
342 production rates of up to 30 ion-pairs $\text{cm}^{-3}\text{s}^{-1}$ during some measurement periods. In urban zones,
343 corona discharge may generate high concentrations of small ions as well. Small ion
344 concentrations of up to 10^4 – 10^5 cm^{-3} have been observed near and downwind of high voltage
345 Transmission lines [Carter and Johnson, 1988; Suda and Sunaga, 1990]. Under favorable
346 conditions, these localized ion sources may lead to the formation of large concentrations of
347 ultrafine particles. In-situ measurements indicate that $[\text{H}_2\text{SO}_4]$ can reach as high as 2×10^8 cm^{-3} in
348 Atlanta, Georgia [McMurry et al., 2005]. Higher ion production rates coupled with higher

349 [H₂SO₄] can lead to significant nucleation, even when the concentration of pre-existing particles
350 is very high (see the top curve in Fig. 4).

351 The effect of ionization rate on aerosol production in the troposphere may have important
352 implications to the possible mechanisms amplifying the impact of solar variations on Earth's
353 climate [Yu, 2002]. During a solar cycle, the values of Q vary by ~20-25% in the upper
354 troposphere and ~5-10% in the lower troposphere at high latitudes, and by ~4-7% in the upper
355 troposphere and ~3-5% in the lower troposphere at low latitudes [Ney, 1959]. Such variations in
356 GCR-induced ionization rate associated with solar activities will cause substantial systematic
357 changes in IMN rates which may have important climatic effects [Yu, 2002]. The physically-
358 based IMN mechanism presented in this paper can be applied in global aerosol models to study
359 how solar variations may influence the abundance of climatic effective aerosols. The IMN
360 mechanism can also be applied to study how emission of radioactive species associated with civil
361 and military nuclear activity may affect the atmospheric ionization (especially near the source
362 regions) and thus the new particle formation rate.

363 364 3.5 Surface area of pre-existing particles (S)

365 Figure 5 shows the dependence of steady state IMN rates on the surface area of the pre-
366 existing particles under four ambient conditions. When [H₂SO₄] is fixed, pre-existing particles
367 affect the nucleation by scavenging small ions and pre-critical clusters. The magnitude of the
368 effect depends on the time needed to grow the molecular clusters to critical clusters (t_g) and the
369 lifetime of these clusters due to scavenging by pre-existing particles (t_s). Therefore, the effect of
370 pre-existing particles on J_{IMN} depends not only on concentration or surface area of pre-existing
371 particles, but also on the sizes of critical clusters (controlled by [H₂SO₄], T, and RH) and growth
372 rates of pre-critical clusters (determined mainly by [H₂SO₄] and to a lesser degree by T and RH).

373 Due to the scavenging, apparent J_{IMN} (i.e., nucleation rate calculated at particle sizes larger than
374 critical sizes, for example 3 nm) decreases with increasing sizes where the apparent nucleation
375 rates are calculated. As mentioned earlier, we use the steady state apparent IMN rates across the
376 clusters containing 10 sulfuric molecules (around 1.5 nm) for the conditions that give very small
377 critical size (containing less than 10 sulfuric molecules).

378 It should be noted that the effects of pre-existing particle surface area on atmospheric particle
379 formation rates should be stronger than those shown in Fig. 5 for two reasons: (1) pre-existing
380 particles have a significant effect on $[\text{H}_2\text{SO}_4]$ to which the nucleation rate is very sensitive, (2)
381 observed particles are generally larger than 3 nm, and the scavenging of clusters/particles smaller
382 than 3 nm but larger than critical sizes will enhance the effect of S. One implication of the effect
383 of S on nucleation is that the emission controlling strategy aimed to reduce particulate mass (and
384 thus surface area) may lead to the increase in new particle formation and thus particle number
385 concentration.

386 An additional point to note from Fig. 5 is that nucleation rate can still be very high even
387 when $S > 500 \mu\text{m}^2 \text{cm}^{-3}$ in polluted areas as long as $[\text{H}_2\text{SO}_4]$ is high enough ($> \sim 10^8 \text{cm}^{-3}$).
388 Measurements indicate that $[\text{H}_2\text{SO}_4]$ can reach above 10^8cm^{-3} in polluted urban areas [*McMurry*
389 *et al.*, 2005]. This may explain why nucleation rates can still happen in some highly polluted
390 regions.

391 392 **4. IMN Look-up Table**

393 In order to study aerosol nucleation in the context of 3-dimensional models, the nucleation
394 calculations must be simplified to reduce computing costs. In the past, various versions of
395 parameterizations have been derived for binary, ternary, and ion nucleation. The
396 parameterization formulas become complex and very lengthy as the number of parameters

397 determining nucleation rates increases [Modgil *et al.*, 2005]. Furthermore, it is hard to obtain
398 accurate parameterization for all the possible ranges of input parameters. For example, the ion
399 nucleation rates calculated with the parameterization of Modgil *et al.* [2005] can deviate by more
400 than one order of magnitude from those calculated by the nucleation model under some
401 parameter spaces.

402 Yu [2008] developed an alternative approach – look-up tables – to reduce the computing
403 costs for 3-D nucleation rate calculations. With the pre-generated look-up table and a simple
404 interpolation subroutine, nucleation rates under given conditions can be calculated accurately
405 (compared to the results from full model simulation) and efficiently. One advantage of the look-
406 up table is that it can cover any needed variable ranges and provide nucleation rates with good
407 accuracy for all the parameter spaces. Another advantage is that it is capable of handling five or
408 more input variables, which is difficult to obtain via parameterizations.

409 Here we describe the look-up table of steady state ion-mediated nucleation rates under a wide
410 range of atmospheric conditions. The table is derived by running an updated version of the
411 kinetic IMN model. The tabulated ion-mediated nucleation rates (J_{IMN}) depend on $[\text{H}_2\text{SO}_4]$, RH,
412 T, Q, and S, and thus the look-up table is five-dimensional. The number of sulfuric acid
413 molecules in the critical cluster (n_a^*), the acid mole fraction (AMOLF*, defined as the relative
414 mole fraction of H_2SO_4 in the system of H_2SO_4 and H_2O), and diameter (d^*) of the critical cluster
415 are also included in the look-up table.

416 Table 1 shows the range of each dependent variable dimension, total number of points in
417 each dimension, and values at each point for the look-up table. In the IMN look-up table, T
418 ranges from 190 K to 302 K with a resolution of 2 K and RH ranges from 0.5% to 99.5% with a
419 resolution of 2%. $[\text{H}_2\text{SO}_4]$ ranges from $5 \times 10^5 - 5 \times 10^8 \text{ cm}^{-3}$ with a resolution of 10 values per

420 decade (geometric), Q ranges from 1.5 – 60 ion-pairs $\text{cm}^{-3}\text{s}^{-1}$ with a resolution of 5 values per
 421 decade (geometric), and S ranges from 10 – 1000 $\mu\text{m}^2\text{cm}^{-3}$ with a resolution of 2.5 values per
 422 decade (geometric) plus one point at $S=1 \mu\text{m}^2\text{cm}^{-3}$. These parameter ranges should cover almost
 423 all the possible conditions in the troposphere relevant to atmospheric nucleation. The range and
 424 resolution in each parameter space can be extended in the future if needed. The look-up table is
 425 composed of J , n_a^* , AMOLF^* , and d^* values at $31 \times 57 \times 51 \times 9 \times 7 = 5,677,371$ points, and has a
 426 total size of ~ 50 MB in the text format. The look-up table, along with a FORTRAN code to read
 427 and interpolate the tables, is given in the AGU auxiliary material or electronic data supplements¹.
 428 For quick application, one can obtain J_{IMN} using an online nucleation rate calculator
 429 (<http://www.albany.edu/~yfq/YuOnLineNucleation.html>) developed by the author.

430 For any given values of $[\text{H}_2\text{SO}_4]$, T , RH , Q , and S within the ranges specified in Table 1, J_{IMN}
 431 and properties of critical clusters (n_a^* , AMOLF^* , and d^*) can be obtained using the look-up table
 432 with an efficient multiple-variable interpolation scheme described in the Appendix. In Figures 1-
 433 5, the values of J_{IMN} interpolated from the look-up table ($J_{\text{IMN}}^{\text{LT}}$) are plotted along with those
 434 calculated with the full model ($J_{\text{IMN}}^{\text{FM}}$) and we can see that $J_{\text{IMN}}^{\text{LT}}$ is very close to $J_{\text{IMN}}^{\text{FM}}$ under the
 435 shown conditions. To explore the accuracy of the interpolated values under other conditions, we
 436 randomly generated 30,000 combinations of $[\text{H}_2\text{SO}_4]$, T , RH , Q , and S within the specified
 437 ranges. It should be noted that many of those combinations are very unlikely to happen in the
 438 atmosphere. J_{IMN} is between 10^{-5} and $10^4 \text{ cm}^{-3}\text{s}^{-1}$ in about 18,000 out of these 30,000 conditions.
 439 A comparison of J_{IMN} , n_a^* , AMOLF^* , and d^* interpolated from the look-up table (LT) with those
 440 calculated with full model (FM) are given in Figure 6. The average absolute deviations (AAD)
 441 marked in each panel are defined as,

¹ Supporting materials are available via Web browser or via Anonymous FTP from <ftp://ftp.agu.org/apend/>
 (Username = "anonymous", Password = "guest").

442

$$\text{AAD} = \frac{\sum_1^N \left| \frac{X^{LT} - X^{FM}}{X^{FM}} \right|}{N}$$

443 where $X = J_{\text{IMN}}, n_a^*, \text{AMOLF}^*, \text{ and } d^*$ and N is the total numbers of cases with J_{IMN} between 10^{-5}
 444 and $10^4 \text{ cm}^{-3}\text{s}^{-1}$.

445 It is clear from Figure 6 that the differences between the interpolated values and those
 446 corresponding values calculated with full IMN model are generally within a few percentages
 447 ($\text{AAD} \leq \sim 4\%$). The cases with relatively large deviations are those cases falling into the
 448 parameter spaces where nucleation rates are sensitive to the changes in the parameters (i.e., the
 449 steepest part of curves shown in Figures 1-5). The deviations can be reduced if we increase the
 450 resolution of the look-up table. Considering the current uncertainty in the IMN model [Yu, 2006],
 451 we think that the results from the present look-up table are acceptable.

452 The application of the look-up table significantly reduces the computing time needed to
 453 calculate large numbers of IMN rates, such as required in 3-dimensional modeling. In a unix
 454 workstation we tested, it takes about 0.3 sec CPU time to calculate $J_{\text{IMN}}, n_a^*, \text{AMOLF}^*, \text{ and } d^*$
 455 for 30,000 randomly selected cases using the look-up table while it takes about 2350 sec CPU
 456 time when we use the full IMN mode. Thus, the look-up table reduces the computing time by a
 457 factor of ~ 8000 . The IMN look-up table has been successfully incorporated into a global
 458 chemical transport model [Yu *et al.*, 2008; Yu and Luo, 2009] and the nucleation rate calculation
 459 has a very small effect on the overall global simulation computing time.

460
 461 **5. Summary**

462 The primary mechanisms of particle nucleation – which control aerosol number
 463 concentrations to a significant degree – remain elusive, despite decades of intensive study. An
 464 ion-mediated nucleation (IMN) mechanism based on a kinetic model, which incorporates new

465 thermodynamic data and physical algorithms and explicitly treats the evaporation of neutral and
466 charged clusters, is supported by long-term measurements of cluster ion spectrum evolution
467 during nucleation events and the excess charge on freshly nucleated particles. With the kinetic
468 IMN model that explicitly resolves the size-dependent microphysical processes among precursor
469 gases and charged and neutral clusters/particles ranging from molecular sizes to several
470 micrometers, we systematically investigate the key parameters controlling IMN rate (J_{IMN}).

471 We show that sulfuric acid vapor concentration ($[\text{H}_2\text{SO}_4]$), temperature (T), relative humidity
472 (RH), ionization rate (Q), and surface area of pre-existing particles (S) have profound and non-
473 linear impacts on J_{IMN} . Generally, J_{IMN} is larger when $[\text{H}_2\text{SO}_4]$ and RH are higher, and T and S
474 are lower. J_{IMN} generally increases with Q unless Q is large and $[\text{H}_2\text{SO}_4]$ is relatively small. With
475 other parameters fixed, J_{IMN} may be insensitive to some parameters under certain conditions
476 when J_{IMN} is limited by other parameter(s). According to the IMN mechanism, T and $[\text{H}_2\text{SO}_4]$
477 are the two most important factors controlling the start and end of nucleation events, although
478 other parameters also contribute to the changes in nucleation rates. The implications of such
479 dependences are discussed. The critical impact of T and $[\text{H}_2\text{SO}_4]$ on J_{IMN} may explain the general
480 occurrence of nucleation in the morning hours and peak of nucleation frequency in the Spring
481 and Fall. More importantly, systematic changes in T and $[\text{H}_2\text{SO}_4]$ associated with future climate
482 and emission changes may substantially affect nucleation rates and aerosol indirect radiative
483 forcing and thus may imply important climate feedback mechanisms. In addition, the dependence
484 of J_{IMN} on ionization rates may provide a physical mechanism amplifying the effect of solar
485 variations on Earth's climate.

486 An IMN look-up table derived using the most recent version of the IMN model is presented.
487 The look-up table is five-dimensional with the key parameters covering almost all the

488 tropospheric conditions relevant to atmospheric nucleation. With the look-up table and a
 489 multiple-variable interpolation subroutine, one can calculate the IMN rates and the properties of
 490 critical clusters under given conditions efficiently and accurately. The usage of the look-up table
 491 reduces the computational costs of the IMN rate calculations by a factor of ~ 8000 and requires
 492 negligible computing resources in multi-dimensional simulations.

493
 494 **Appendix. Multi-variable linear interpolation scheme**

495 The tabulated ion-mediated nucleation rates (J_{IMN}) depend on $[\text{H}_2\text{SO}_4]$, RH, T, Q, and S, and
 496 thus the look-up table is five-dimensional. The properties of critical clusters (n_a^* , AMOLF*, and
 497 d^*) depend on $[\text{H}_2\text{SO}_4]$, RH, and T, and thus the corresponding look-up table is three-
 498 dimensional. For any set of $[\text{H}_2\text{SO}_4]$, RH, T, Q, and S, J_{IMN} along with n_a^* , AMOLF*, and d^*
 499 can be calculated efficiently based on a multiple-variable linear interpolation scheme described
 500 below. We use J_{IMN} as example.

501 Let $x=[\text{H}_2\text{SO}_4]$, $y=\text{RH}$, $z=\text{T}$, $u=\text{Q}$, $v=\text{S}$, and $J=J_{\text{IMN}}$, then $J=f(x, y, z, u, v)$. To find J_0 value
 502 at the point $(x_0, y_0, z_0, u_0, v_0)$, we first need to locate the closest set of grid points surrounding the
 503 point $(x_0, y_0, z_0, u_0, v_0)$ in each look-up table dimension: $x_1 \leq x_0 < x_2$; $y_1 \leq y_0 < y_2$; $z_1 \leq z_0 < z_2$; $u_1 \leq u_0 < u_2$;
 504 $v_1 \leq v_0 < v_2$. The values of points of look-up table given in Table 1 are designed in a way that x_1 , x_2 ,
 505 y_1 , y_2 , z_1 , z_2 , u_1 , u_2 , v_1 , and v_2 can be determined quickly with a simple calculation (based on the
 506 analytical formula given in the last column of Table 1).

507 (1) Linear interpolation: $J=f(x)$.

508 Let $J_1=f(x_1)$, $J_2=f(x_2)$, and $dx=x_2-x_1$, $dx_1=x_0-x_1$, $dx_2=x_2-x_0$, then

$$509 \quad J_0=f(x_0)=J_1+(J_2-J_1)dx_1/dx=(J_1 dx_2+J_2 dx_1)/dx \quad (\text{A1})$$

510 (2) Bi-linear interpolation: $J=f(x, y)$.

511 For any given point (x_0, y_0) , there are $2^2=4$ surrounding points. Let $J_{11} = f(x_1, y_1)$, $J_{12} = f(x_1,$
 512 $y_2)$, $J_{21} = f(x_2, y_1)$, $J_{22} = f(x_2, y_2)$, $dy=y_2-y_1$, $dy_1=y_0-y_1$, $dy_2=y_2-y_0$.

513 First, obtain J_{10} and J_{20} based on linear interpolation (Eq. A1),

$$514 J_{10} = f(x_1, y_0) = (J_{11} dy_2 + J_{12} dy_1)/dy$$

$$515 J_{20} = f(x_2, y_0) = (J_{21} dy_2 + J_{22} dy_1)/dy$$

516 Then use linear interpolation (Eq. A1) again to get

$$517 J_{00} = f(x_0, y_0) = (J_{10} dx_2 + J_{20} dx_1)/dx = (J_{11} dx_2 dy_2 + J_{12} dx_2 dy_1$$

 518 $+ J_{21} dx_1 dy_2 + J_{22} dx_1 dy_1)/(dx dy) \quad (A2)$

519 (3) Tri-linear interpolation: $J = f(x, y, z)$.

520 For any given point (x_0, y_0, z_0) , there are $2^3=8$ surrounding points. Let $J_{111} = f(x_1, y_1, z_1)$, J_{112}
 521 $= f(x_1, y_1, z_2)$, \dots , $J_{221} = f(x_2, y_2, z_1)$, $J_{222} = f(x_2, y_2, z_2)$, $dz=z_2-z_1$, $dz_1=z_0-z_1$, $dz_2=z_2-z_0$. We can
 522 get $J_{000}=(x_0, y_0, z_0)$ by reducing the tri-linear interpolation to bi-linear interpolation.

523 First, get J_{110} , J_{120} , J_{210} , J_{220} based on Eq. (A1):

$$524 J_{110} = f(x_1, y_1, z_0) = (J_{111} dz_2 + J_{112} dz_1)/dz$$

$$525 J_{120} = f(x_1, y_2, z_0) = (J_{121} dz_2 + J_{122} dz_1)/dz$$

$$526 J_{210} = f(x_2, y_1, z_0) = (J_{211} dz_2 + J_{212} dz_1)/dz$$

$$527 J_{220} = f(x_2, y_2, z_0) = (J_{221} dz_2 + J_{222} dz_1)/dz$$

528 Then, obtain $J_{000}=(x_0, y_0, z_0)$ with Eq. (A2),

$$529 J_{000} = (J_{111} dx_2 dy_2 dz_2 + J_{112} dx_2 dy_2 dz_1 + \dots J_{221} dx_1 dy_1 dz_2 + J_{222} dx_1 dy_1 dz_1)/(dx dy dz) \quad (A3)$$

530 (4) Multi-variable linear interpolation

531 The above derivation of linear interpolation can be generalized to a system with N variables.

532 The strategy is to reduce the number of variables by 1 with Eq. A1, and then apply (N-1)-linear
 533 interpolation formula to get the final interpolation expression.

534 For the 5-D look-up table $J = f(x,y,z,u,v)$, there are $2^5=32$ grid points surrounding any given
 535 point $(x_0, y_0, z_0, u_0, v_0)$. The formula for determining $J_{00000} = f(x_0,y_0,z_0,u_0,v_0)$ can be expressed as,

$$536 \quad J_{00000} = (J_{11111} dx_2 dy_2 dz_2 du_2 dv_2 + J_{11112} dx_2 dy_2 dz_2 du_2 dv_1 \\ 537 \quad + \dots J_{22221} dx_1 dy_1 dz_1 du_1 dv_2 + J_{22222} dx_1 dy_1 dz_1 du_1 dv_1) / (dx dy dz du dv) \quad (A4)$$

538 where $J_{11111} = f(x_1, y_1, z_1, u_1, v_1)$, $J_{11112} = f(x_1, y_1, z_1, u_1, v_2)$, \dots , $J_{22221} = f(x_2, y_2, z_2, u_2, v_1)$, J_{22222}
 539 $= f(x_2, y_2, z_2, u_2, v_2)$, $du=u_2-u_1$, $du_1=u_0-u_1$, $du_2=u_2-u_0$, $dv=v_2-v_1$, $dv_1=v_0-v_1$, $dv_2=v_2-v_0$.

540
 541 **Acknowledgments.** This study is supported by NSF under grant 0618124, NASA under grant
 542 NNX08AK48G, and NOAA under grant NA05OAR4310103.

543
 544 **References**

- 545 Albrecht, B. A. (1989), Aerosols, cloud microphysics and fractional cloudiness, *Sciences*, 245,
 546 1227-1230.
- 547 Arnold, F. (1980), Multi-ion complexes in the stratosphere—Implications for trace gases and
 548 aerosol, *Nature*, 284, 610-611.
- 549 Boy, M., J. Kazil, E.R. Lovejoy, A. Guenther, M. Kulmala (2008), Relevance of ion-induced
 550 nucleation of sulfuric acid and water in the lower troposphere over the boreal forest at
 551 northern latitudes, *Atmospheric Research*, 90,151–158.
- 552 Carter, P. J., and G. B. Johnson (1988), Space charge measurements downwind from a
 553 monopolar 500 kV HVDC test line, *IEEE Transactions on Power Delivery*, 3, 2056 -2063.
- 554 Castleman, A. W., Jr., P. M. Holland, & R. G. Keesee (1978), The properties of ion clusters and
 555 their relationship to heteromolecular nucleation, *J. Chem. Phys.*, 68, 1760-1767.

- 556 Chan, L. Y., and V. A. Mohnen (1980), The formation of ultrafine ion H₂O-H₂SO₄ aerosol
557 particles through ion-induced nucleation process in the stratosphere, *J. Aerosol. Sci.*, *11*, 35-
558 45, 1980.
- 559 Charlson, R. J., J.E. Lovelock, M. O. Andreae, and S.G. Warren (1987), Oceanic phytoplankton,
560 atmospheric sulphur, cloud albedo and climate, *Nature*, *326*, 655–661.
- 561 Dhanorkar, S., A. K. Kamra (1994), Diurnal variation of ionization rate close to ground, *J.*
562 *Geophys. Res.*, *99*, 18523-18526, 10.1029/94JD01335.
- 563 Eisele, F. L., et al. (2006), Negative atmospheric ions and their potential role in ion-induced
564 nucleation, *J. Geophys. Res.*, *111*, D04305, doi:10.1029/2005JD006568.
- 565 Froyd, K. D. (2002), *Ion induced nucleation in the atmosphere: Studies of NH₃, H₂SO₄, and H₂O*
566 *cluster ions*, Ph.D. thesis, Univ. of Colo., Boulder.
- 567 Gagné, S., L. Laakso, T. Petäjä, V.-M. Kerminen, and M. Kulmala (2008), Analysis of one year
568 of Ion-DMPS data from the SMEAR II station, Finland, *Tellus B*, *60*, 318–329.
- 569 Hamill, P., R. P. Turco, C. S. Kiang, O. B. Toon, and R. C. Whitten (1982), An analysis of
570 various nucleation mechanisms for sulfate particles in the stratosphere, *J. Aerosol Sci.*, *13*,
571 561-585.
- 572 Hirsikko, A., et al. (2007), Identification and classification of the formation of intermediate ions
573 measured in boreal forest, *Atmos. Chem. Phys.*, *7*, 201-210.
- 574 Iida, K., et al. (2006), Contribution of ion-induced nucleation to new particle formation:
575 Methodology and its application to atmospheric observations in Boulder, Colorado, *J.*
576 *Geophys. Res.*, *111*, D23201, doi:10.1029/2006JD007167.
- 577 IPCC (2007), *Climate Change 2007: The Physical Scientific Basis*, edited by S. Solomon, D.
578 Qin, et al., Cambridge Univ. Press, New York.

- 579 Kazil, J. and Lovejoy, E. R. (2007) A semi-analytical method for calculating rates of new sulfate
580 aerosol formation from the gas phase, *Atmos. Chem. Phys.*, 7, 3447-3459.
- 581 Kulmala, M., et al. (2004a), Formation and growth rates of ultrafine atmospheric particles: A
582 review of observations, *J. Aerosol Sci.*, 35, 143–176.
- 583 Kulmala, M., et al. (2004b), Initial steps of aerosol growth, *Atmos. Chem. Phys.*, 4, 2553-2560.
- 584 Kulmala, M., I. Riipinen, M. Sipilä, et al. (2007), Toward direct measurement of atmospheric
585 nucleation, *Science*, 318, 89-92.
- 586 Laakso, L., J. M. Mäkelä, L. Pirjola, and M. Kulmala (2003), Model studies of ion-induced
587 nucleation in the atmosphere, *J. Geophys. Res.*, 107, 4427, doi:10.1029/2002JD002140.
- 588 Laakso, L., et al. (2007), Detecting charging state of ultra-fine particles: instrumental
589 development and ambient measurements, *Atmos. Chem. Phys.*, 7, 1333-1345.
- 590 Laaksonen, A., et al. (2008), The role of VOC oxidation products in continental new particle
591 formation, *Atmos. Chem. Phys.*, 8, 2657-2665.
- 592 Lovejoy, E. R., J. Curtius, and K. D. Froyd (2004), Atmospheric ion-induced nucleation of
593 sulfuric acid and water, *J. Geophys. Res.*, 109, D08204, doi:10.1029/2003JD004460.
- 594 Manninen, H. E., Nieminen, T., Riipinen, I., et al. (2009), Charged and total particle formation
595 and growth rates during EUCAARI 2007 campaign in Hyytiälä, *Atmos. Chem. Phys.*
596 *Discuss.*, 9, 5119-5151.
- 597 McMurry, P. H., et al. (2005), A criterion for new particle formation in the sulfur-rich Atlanta
598 atmosphere, *J. Geophys. Res.*, 110, D22S02, doi:10.1029/2005JD005901.
- 599 Minschwaner, K., and A. E. Dessler (2004), Water vapor feedback in the tropical upper
600 troposphere: Model results and observations, *J. of Climate*, 17, 1272-1282.

- 601 Modgil, M. S., S. Kumar, S. N. Tripathi, and E. R. Lovejoy (2005), A parameterization of ion-
602 induced nucleation of sulphuric acid and water for atmospheric conditions, *J. Geophys. Res.*,
603 *110*, D19205, doi:10.1029/2004JD005475.
- 604 Nadykto, A., and F. Yu (2003), Uptake of neutral polar vapour molecules by charged particles:
605 Enhancement due to dipole-charge interaction, *J. Geophys. Res.*, *108*(D23), 4717,
606 doi:10.1029/2003JD003664.
- 607 Ney, E. P. (1959), Cosmic radiation and the weather, *Nature*, *183*, 451-452.
- 608 O'Dowd, C. D., et al. (2008), Airborne measurements of nucleation mode particles II: boreal
609 forest nucleation events, *Atmos. Chem. Phys. Discuss.*, *8*, 2821-2848.
- 610 Raes, F., Augustin, J., & Vandingenen R. (1986), The role of ion-induced aerosol formation in
611 the lower atmosphere. *J. Aerosol Sci.*, *17*, 466-470.
- 612 Reiter, R. (1992), *Phenomena in Atmospheric and Environmental Electricity*, Elsevier, New
613 York.
- 614 Stanier, C., A. Khlystov, and S. N. Pandis (2004), Nucleation events during the Pittsburgh Air
615 Quality Study: Description and relation to key meteorological, gas phase, and aerosol
616 parameters, *Aerosol Sci. Technol.*, *38*, suppl. 1, 253–264.
- 617 Suda, T., and Y. Sunaga (1990), An experimental study of large ion density under the Shiobara
618 HVDC test line, *IEEE Trans Power Delivery*, *5*, 1426-1435.
- 619 Twomey, S. (1977), The influence of pollution on the shortwave albedo of clouds, *J. Atmos. Sci.*,
620 *34*, 1149-1152.
- 621 Vartiainen, E., et al. (2007), Ion and particle number concentrations and size distributions along
622 the Trans-Siberian railroad, *Boreal Env. Res.*, *12*, 375-396.

- 623 Weber, R. J., et al. (2003), New particle formation in anthropogenic plumes advecting from Asia
624 observed during TRACE-P, *J. Geophys. Res.*, *108*(D21), 8814, doi:10.1029/2002JD003112.
- 625 Wilhelm, S., Eichkorn, S., Wiedner, D., Pirjola, L., & Arnold (2004), F. Ion-induced aerosol
626 formation: new insights from laboratory measurements of mixed cluster ions,
627 $\text{HSO}_4^- (\text{H}_2\text{SO}_4)_a (\text{H}_2\text{O})_w$ and $\text{H}^+ (\text{H}_2\text{SO}_4)_a (\text{H}_2\text{O})_w$, *Atmos. Environ.*, *38*, 1735-1744.
- 628 Yu, F. (2002), Altitude variations of cosmic ray induced production of aerosols: Implications for
629 global cloudiness and climate, *J. Geophys. Res.*, *107*(A7), 10.1029/2001JA000248.
- 630 Yu, F. (2005), Modified Kelvin-Thomson equation considering ion-dipole interaction:
631 Comparison with observed ion-clustering enthalpies and entropies, *J. Chem. Phys.*, *122*,
632 084503.
- 633 Yu, F. (2006), From molecular clusters to nanoparticles: Second-generation ion-mediated
634 nucleation model, *Atmos. Chem. Phys.*, *6*, 5193-5211, 2006.
- 635 Yu, F. (2007), An improved quasi-unary nucleation model for binary H_2SO_4 - H_2O homogeneous
636 nucleation, *J. Chem. Phys.*, *127*, 054301.
- 637 Yu, F. (2008), Updated H_2SO_4 - H_2O binary homogeneous nucleation rate look-up tables, *J.*
638 *Geophys. Res.*, *113*, D24201, doi:10.1029/2008JD010527.
- 639 Yu, F., and R. P. Turco (1997), The role of ions in the formation and evolution of particles in
640 aircraft plumes, *Geophys. Res. Lett.*, *24*, 1927-1930.
- 641 Yu, F., and R. P. Turco (2000), Ultrafine aerosol formation via ion-mediated nucleation,
642 *Geophys. Res. Lett.*, *27*, 883-886.
- 643 Yu, F., and R. P. Turco (2001), From molecular clusters to nanoparticles: The role of ambient
644 ionization in tropospheric aerosol formation, *J. Geophys. Res.*, *106*, 4797-4814.

645 Yu, F., and R. P. Turco (2007), Charging State of Freshly Nucleated Particles: Implication for
646 Nucleation Mechanisms, in *Nucleation and Atmospheric Aerosols*, C. D. O'Dowd and P. E.
647 Wagner (eds.), p392-396, Springer 2007.

648 Yu, F., and R. P. Turco (2008), Case studies of particle formation events observed in boreal
649 forests: Implications for nucleation mechanisms, *Atmos. Chem. Phys.*, 8, 6085-6102.

650 Yu, F., et al. (2007), Interactive comment on “Ion-mediated nucleation as an important global
651 source of tropospheric aerosols”, *Atmos. Chem. Phys. Discuss.*, 7, S6602–S6608, 2007.
652 www.atmos-chem-phys-discuss.net/7/S6602/2007/

653 Yu, F., Z. Wang, G. Luo, and R. P. Turco (2008), Ion-mediated nucleation as an important
654 source of tropospheric aerosols, *Atmos. Chem. Phys.*, 8, 2537-2554.

655 Yu, F., and G. Luo (2009), Simulation of particle size distribution with a global aerosol model:
656 Contribution of nucleation to aerosol and CCN number concentrations, *Atmos. Chem. Phys.*
657 *Discuss.*, 9, 10597-10645.

658 _____
659 F. Yu, Atmospheric Sciences Research Center, State University of New York at Albany, 251
660 Fuller Road, Albany, New York 12203. (yfq@asrc.cestm.albany.edu)

661

662

663 **Figure Captions:**

664 **Figure 1.** Ion-mediated nucleation rate as a function of sulfuric acid vapor concentration
 665 ($[\text{H}_2\text{SO}_4]$) under four different ambient conditions, calculated with the full IMN model (solid
 666 lines) and IMN look-up table (dashed lines). In the legend, read T295Q10RH50S100 as $T=295\text{K}$,
 667 $Q=10$ ion-pairs $\text{cm}^{-3}\text{s}^{-1}$, $\text{RH}=50\%$, and $S=100 \mu\text{m}^2 \text{cm}^{-3}$.

668
 669 **Figure 2.** The dependence of predicted ion-mediated nucleation rate on T for four different
 670 ambient conditions, based on the full IMN model (solid lines) and IMN look-up table (dashed
 671 lines). In the legend, read A3E7Q10RH50S100 as $[\text{H}_2\text{SO}_4]=3\times 10^7 \text{cm}^{-3}$, $Q=10$ ion-pairs $\text{cm}^{-3}\text{s}^{-1}$,
 672 $\text{RH}=50\%$, and $S=100 \mu\text{m}^2 \text{cm}^{-3}$.

673
 674 **Figure 3.** The dependence of predicted IMN rate on RH under four selected conditions, based on
 675 the full IMN model (solid lines) and IMN look-up table (dashed lines). In the legend, read
 676 A1E7T275Q10S50 as $[\text{H}_2\text{SO}_4] = 3\times 10^7 \text{cm}^{-3}$, $Q=10$ ion-pairs $\text{cm}^{-3}\text{s}^{-1}$, $T=275 \text{K}$, and $S=50 \mu\text{m}^2$
 677 cm^{-3} .

678
 679 **Figure 4.** The dependence of predicted IMN rates on Q under four selected conditions, based on
 680 the full IMN model (solid lines) and IMN look-up table (dashed lines). In the legend, read
 681 A1E7T275RH50S50 as $[\text{H}_2\text{SO}_4]=3\times 10^7 \text{cm}^{-3}$, $Q=10$ ion-pairs $\text{cm}^{-3}\text{s}^{-1}$, $T=275 \text{K}$, $\text{RH}=50\%$, and
 682 $S=50 \mu\text{m}^2 \text{cm}^{-3}$.

683
 684 **Figure 5.** The dependence of predicted IMN rates on S under four selected conditions, based on
 685 the full IMN model (solid lines) and IMN look-up table (dashed lines). In the legend, read
 686 A1E7T275Q10RH50 as $[\text{H}_2\text{SO}_4]=3\times 10^7 \text{cm}^{-3}$, $Q=10$ ion-pairs $\text{cm}^{-3}\text{s}^{-1}$, $T=275 \text{K}$, and $\text{RH}=50 \%$.

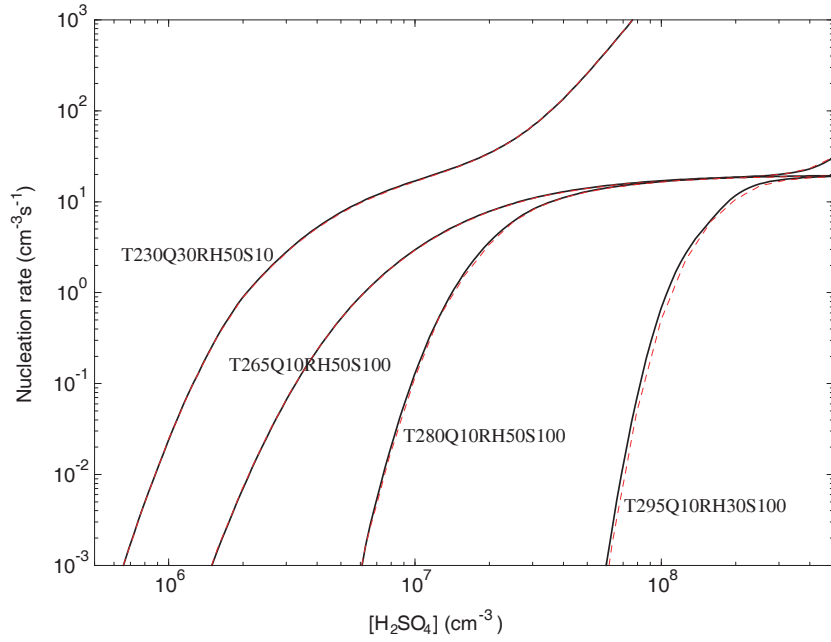
687

688 **Figure 6.** Comparisons of J_{IMN} , n_a^* , AMOLF^* , and d^* interpolated from the IMN look-up table
 689 with those calculated with full IMN model. See text for the definition of the average absolute
 690 deviations (AAD) given in each panel.

691
 692 **Table 1.** The range of each dependent variable dimension, the total number of points in each
 693 dimension, and the values at each point for the IMN look-up table.

	Range	Total # of points	Values at each point
$[\text{H}_2\text{SO}_4]$ (cm^{-3})	$5 \times 10^5 - 5 \times 10^8$	31	$[\text{H}_2\text{SO}_4](i) = 5 \times 10^5 \times 10^{(i-1)/10}$, $i = 1, 31$
T (K)	190 – 302	57	$T(j) = 190 + 2 \times (j - 1)$, $j = 1, 57$
RH (%)	0.5 – 99.5	51	RH(1)=0.5, RH(k) = $2 \times (k-1)$, $k=2, 50$; RH(51)=99.5
Q (ion-pairs $\text{cm}^{-3}\text{s}^{-1}$)	1.5 – 60	9	$Q(l) = 1.5 \times 10^{(l-1)/5}$, $l = 1, 9$
S ($\mu\text{m}^2\text{cm}^{-3}$)	1 – 1000	7	$S(1)=1$, $S(m) = 10 \times 10^{(m-2)/2.5}$, $m = 2, 7$

694
 695
 696

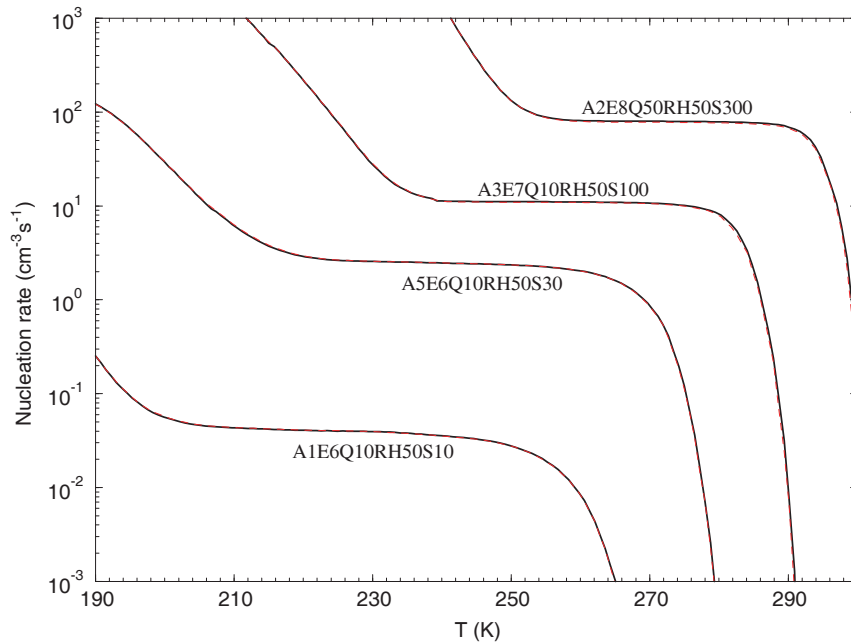


697
698
699
700

Yu, JGR, Figure 1

701

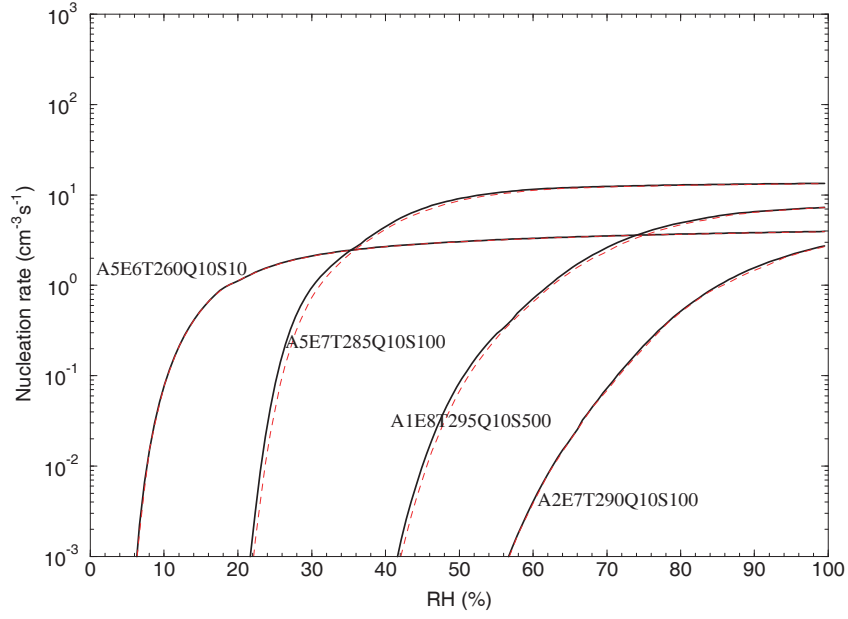
702



703
704

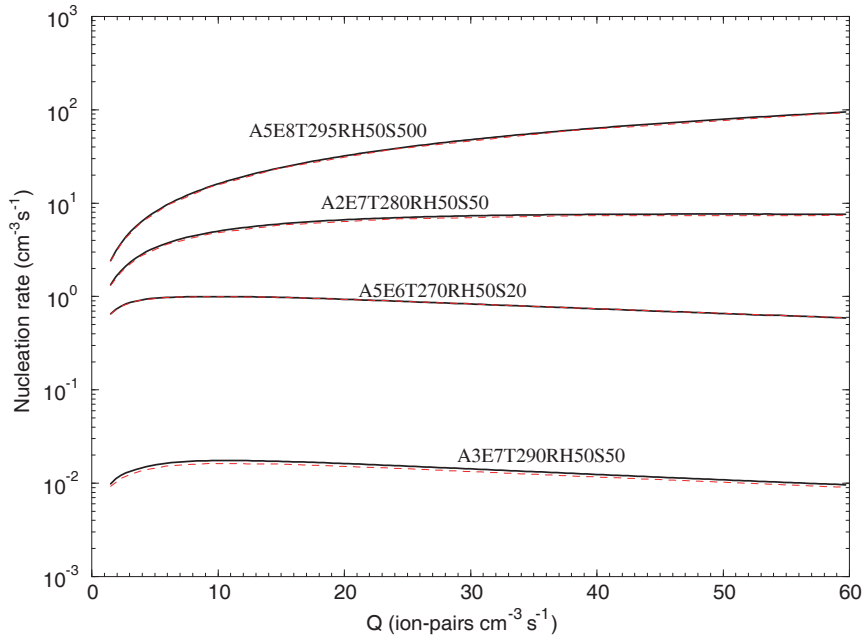
Yu, JGR, Figure 2

705
706



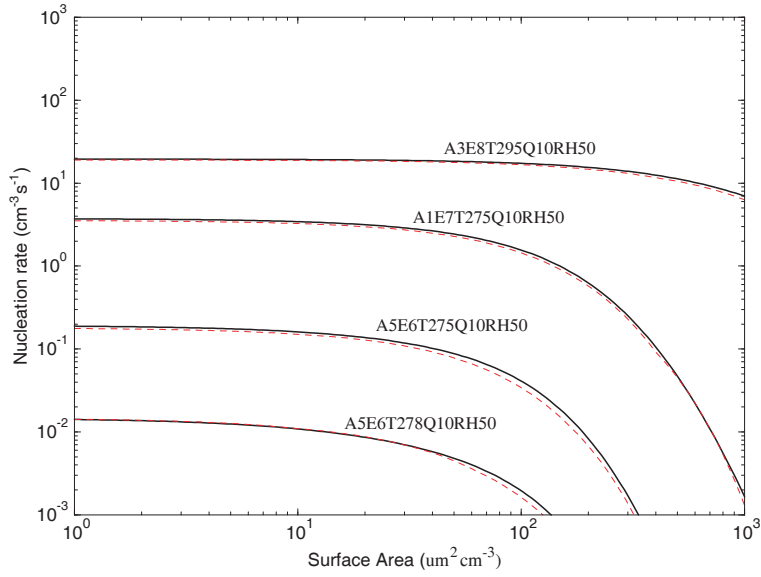
707
708
709
710
711

Yu, JGR, Figure 3



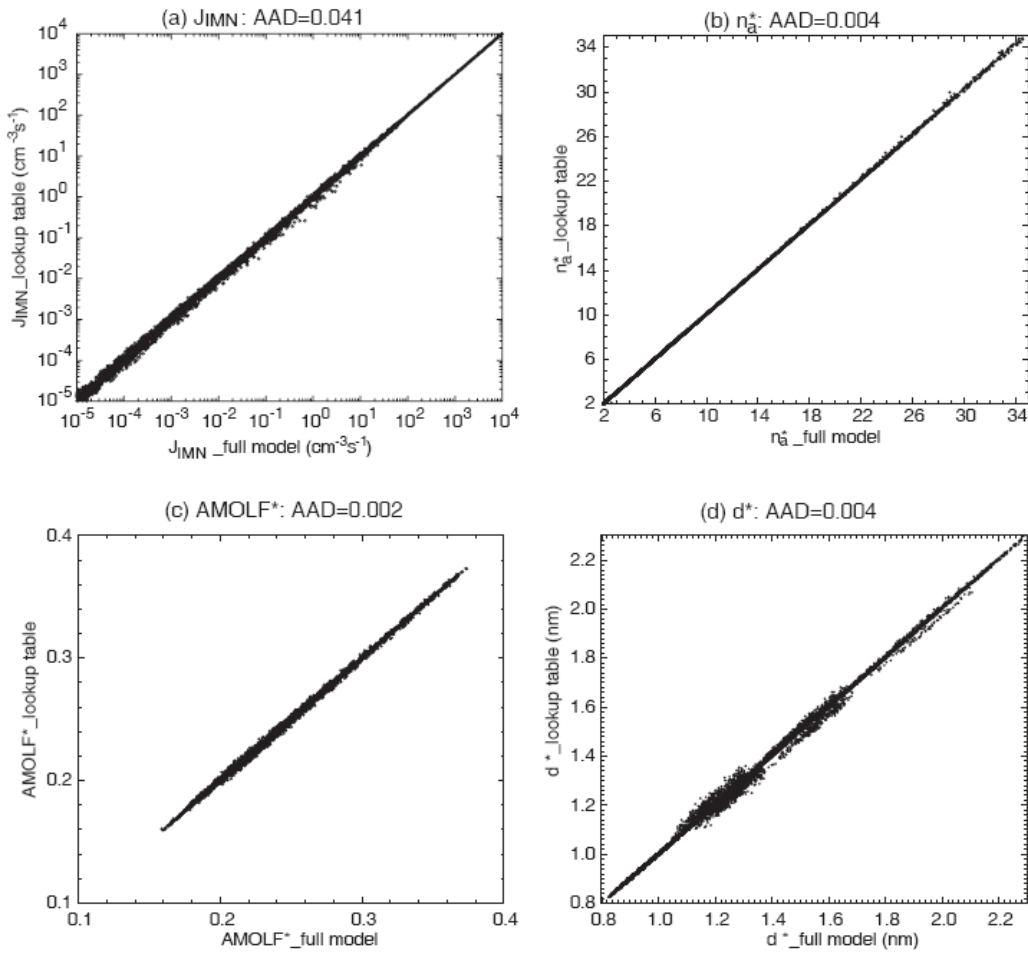
712
713
714
715

Yu, JGR, Figure 4



Yu, JGR, Figure 5

716
717
718
719



Yu, JGR, Figure 6

720
721